



UNIVERSITY OF LEEDS

This is a repository copy of *Evaporite weathering and deposition as a long-term climate forcing mechanism*.

White Rose Research Online URL for this paper:  
<https://eprints.whiterose.ac.uk/167333/>

Version: Accepted Version

---

**Article:**

Shields, GA and Mills, BJW [orcid.org/0000-0002-9141-0931](https://orcid.org/0000-0002-9141-0931) (2021) Evaporite weathering and deposition as a long-term climate forcing mechanism. *Geology*, 49 (3). pp. 299-303. ISSN 0091-7613

<https://doi.org/10.1130/G48146.1>

---

© 2020 Geological Society of America. This is an author produced version of an article published in *Geology*. Uploaded in accordance with the publisher's self-archiving policy.

**Reuse**

Items deposited in White Rose Research Online are protected by copyright, with all rights reserved unless indicated otherwise. They may be downloaded and/or printed for private study, or other acts as permitted by national copyright laws. The publisher or other rights holders may allow further reproduction and re-use of the full text version. This is indicated by the licence information on the White Rose Research Online record for the item.

**Takedown**

If you consider content in White Rose Research Online to be in breach of UK law, please notify us by emailing [eprints@whiterose.ac.uk](mailto:eprints@whiterose.ac.uk) including the URL of the record and the reason for the withdrawal request.



[eprints@whiterose.ac.uk](mailto:eprints@whiterose.ac.uk)  
<https://eprints.whiterose.ac.uk/>

# 1 **Evaporite weathering and deposition as a long-term climate forcing**

2  
3 Graham A. Shields<sup>1\*</sup> and Benjamin J.W. Mills<sup>2</sup>

4  
5 <sup>1</sup>Department of Earth Sciences, University College London, Gower Street, London WC1E 6BT, UK;

6 \*corresponding author: g.shields@ucl.ac.uk

7 <sup>2</sup>School of Earth and Environment, University of Leeds, Leeds LS2 9JT, UK

## 8 9 **Abstract**

10 Although it is widely accepted that Earth's long-term surface temperature is regulated by the  
11 mutual dependence of silicate weathering and climate on CO<sub>2</sub>, the root causes of some climatic  
12 events remain unresolved. We show here for the first time that imbalances between evaporite  
13 weathering and deposition can affect climate through the process of carbonate sedimentation.  
14 Calcium sulfate weathering supplies Ca<sup>2+</sup> ions to the ocean unaccompanied by carbonate  
15 alkalinity, so that increased carbonate precipitation strengthens greenhouse forcing through  
16 transfer of CO<sub>2</sub> to the atmosphere. Conversely, calcium sulfate deposition weakens greenhouse  
17 forcing, while the high depositional rates of evaporite giants may overwhelm the silicate  
18 weathering feedback, causing several degrees of planetary cooling. Non-steady state evaporite  
19 dynamics and related feedbacks have hitherto been overlooked as drivers of long-term carbon  
20 cycle change. Here we illustrate the importance of evaporite deposition, in particular, by  
21 showing how a series of massive depositional events contributed to global cooling during the  
22 mid-late Miocene.

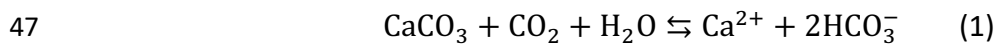
## 23 24 25 **Introduction**

26 “Carbon dioxide partial pressure and Earth's greenhouse effect are ... buffered by the  
27 temperature dependence of the rate of carbon dioxide consumption in the weathering of silicate  
28 minerals” (Walker et al., 1981). This canonical negative feedback is still our best explanation  
29 for how Earth's long-term surface temperature resists external forcing, such as changes in solar  
30 luminosity or CO<sub>2</sub> outgassing. However, despite broad agreement around the operation of  
31 Earth's natural thermostat, some features of Earth's climate history, notably abrupt  
32 hyperthermal or cooling events, imply weakening of the silicate weathering buffer.

33

34 One inherent assumption of the silicate weathering feedback is that the calcium input to the  
35 ocean is balanced by carbonate deposition on long time scales, i.e.  $>10^5$  years. The  
36 stoichiometric equivalence between the Ca (and Mg) (Berner, 1991) released from silicate  
37 weathering and the Ca removed through carbonate deposition has long been known to buffer  
38 the long-term carbon cycle (Berner, 2012). However, the riverine Ca + Mg dissolved load  
39 integrates contributions from three different lithologies: carbonates, silicates and evaporites,  
40 which have contrasting effects on the carbon cycle (Figure 1 and Equations 1-3). Carbonate  
41 minerals dissolve quantitatively (Eq. 1), and release calcium ions and carbonate alkalinity to  
42 the ocean, with one mole of bicarbonate sourced from the rock reservoir and one from the  
43 atmosphere. Although carbonate weathering transfers  $\text{CO}_2$  from the atmosphere to the ocean,  
44 it does not affect the long-term carbon balance because subsequent carbonate burial (reverse  
45 of Eq. 1) effectively recombines these constituents and releases  $\text{CO}_2$ .

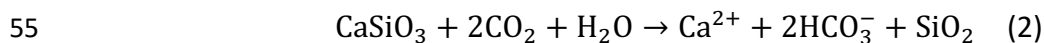
46



48

49 Silicate minerals undergo incongruent leaching during chemical weathering (Eq. 2), resulting  
50 in the release of cations and carbonate alkalinity to the ocean, but with carbon entirely derived  
51 from the atmosphere. This drawdown of  $\text{CO}_2$  exceeds that released during carbonate  
52 precipitation, and thus coupled silicate weathering and carbonate burial results in a net transfer  
53 of carbon from the surface system into the sediments.

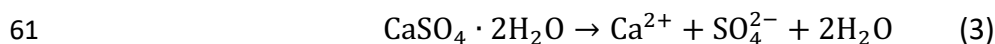
54



56

57 Finally, non-carbonate evaporite minerals like gypsum (Eq. 3) dissolve rapidly and entirely,  
58 releasing cations (e.g.  $\text{Na}^+$ ,  $\text{Mg}^{2+}$ ,  $\text{Ca}^{2+}$ ,  $\text{K}^+$ ) and anions (halides, sulfates) into rivers  
59 unaccompanied by carbonate alkalinity, for example:

60



62

63 In established long-term biogeochemical models (Berner, 1991; Lenton et al., 2018; Mills et  
64 al., 2018), evaporite fluxes are negated by assuming a close balance between the weathering  
65 and deposition of Ca- and Mg-bearing evaporite minerals on all time scales. However, the  
66 largest, basin-scale or giant evaporite deposits formed sporadically due to the restriction of  
67 marginal ocean basins, most commonly during basin closure or rifting (Warren, 2010). Unlike

68 carbonate or silicate lithologies, evaporites are also unevenly distributed geographically and  
69 are of variable chemical and mineralogical composition, meaning that the relative contribution  
70 of evaporites to global Ca and Mg fluxes varied greatly over Earth history (Wortmann and  
71 Paytan, 2012). Due to the regional distribution of rare evaporite giant deposits, imbalance  
72 between evaporite, and specifically calcium sulfate, weathering and deposition must have  
73 occurred on up to  $10^7$ -year time scales since the onset of oxidative pyrite weathering after the  
74 Great Oxidation Event.

75

### 76 **Evaporite giant deposition and weathering during the Cenozoic Era**

77 The last evaporite giant formed episodically between 5.97 and 5.33 million years ago  
78 (Meilijson et al., 2019) due to restriction of the Mediterranean Sea during the Messinian  
79 Salinity Crisis (MSC). The MSC followed evaporite deposition in the Red Sea during the  
80 preceding Tortonian Age and brought to an end evaporite deposition across Eurasia spanning  
81 the entire Miocene Epoch (Rohais et al., 2016; Mandic et al., 2019) (Figure 2). The first giant  
82 evaporite deposits of the Cenozoic Era were particularly gypsum-rich (Al-Juboury and  
83 McCann, 2008), due primarily to precipitation from sulfate-rich seawater (Halevy et al., 2012;  
84 Zeebe and Tyrrell, 2019), and formed as a result of the restriction of the Mesopotamian and  
85 Paratethyan seaways during Langhian (c. 15.97-13.65 Ma) (Al-Juboury and McCann, 2008)  
86 and early Serravalian (c. 13.6-13.0 Ma) (De Leeuw et al., 2010) times, respectively. Miocene  
87 evaporite deposits formed predominantly, therefore, in two episodes (c. 16-13 Ma and c. 9-5  
88 Ma) that delimit the only evaporite giants of the last 120 million years (Warren, 2010).

89 With the exception of these two mid-late Miocene intervals, evaporite weathering likely  
90 outpaced deposition for most of the Cenozoic Era. Moreover exceptionally high rates of  
91 evaporite weathering likely occurred following the initial phase of Himalayan collision in the  
92 early Eocene (Wortmann and Paytan, 2012), which records a rise in seawater  $\delta^{34}\text{S}$  beginning  
93 c. 53 Ma (Yao et al., 2020). This weathering event and the later deposition events are shown in  
94 Figure 2, and are plotted against global average surface temperature as inferred from benthic  
95 foraminiferal oxygen isotopes (Zachos et al., 2008; Hansen et al., 2013). While it is difficult to  
96 constrain the precise timing of evaporite weathering events during the early Eocene, the timings  
97 of evaporite deposition during the Langhian-Serravallian and Tortonian-Messinian are much  
98 better known, and both coincide with episodes of major global cooling and ice sheet expansion  
99 (Holbourn et al., 2018; Bialik et al., 2019).

100

## 101 **Evaporite forcing of climate change**

102 Here we define and demonstrate a mechanism by which massive evaporite events may  
103 contribute to shifts in climate. The events drive non-steady-state marine inventories of calcium,  
104 with implications for the net burial of calcium carbonate, and thus ocean carbonate chemistry.  
105 The saturation state of calcium carbonate,  $\Omega$ , depends on the concentration of  $\text{Ca}^{2+}$  and  $\text{CO}_3^{2-}$   
106 ions:

$$108 \quad \Omega = \frac{[\text{Ca}^{2+}][\text{CO}_3^{2-}]}{K_{sp}} \quad (4)$$

109 where  $K_{sp}$  is the solubility constant, which is sensitive to temperature, pressure and salinity.  
110 Any large increase in the ocean Ca inventory, in the absence of any linked change in alkalinity,  
111 should increase  $\text{CaCO}_3$  burial rates, lower marine pH, and thus release  $\text{CO}_2$  to the atmosphere  
112 (Zeebe and Tyrrell, 2019). Conversely, evaporite deposition causes  $[\text{Ca}]$  to decrease and so  
113 results in reduced carbonate precipitation, rising alkalinity and gas-transfer of  $\text{CO}_2$  into the  
114 ocean. Because global marine carbonate burial rates were decoupled from the carbonate  
115 compensation depth (CCD) during the Cenozoic (Greene et al., 2019), direct comparison with  
116 CCD changes is complex. Ultimately, imbalances in marine alkalinity and  $\text{CaCO}_3$  burial would  
117 be remedied by the response of silicate weathering to changes in  $\text{CO}_2$ , but the intervening  $\sim 10^6$   
118 years could see substantial climatic change.

120  
121 To explore the potential magnitude of the effects of evaporite weathering and burial events on  
122 the long-term carbon cycle we modify a recent biogeochemical box model (Dal Corso et al.,  
123 2020). The model consists of an atmosphere and three ocean boxes (surface, high-latitude,  
124 deep) (Sarmiento and Toggweiler, 1984), has an explicit representation of carbonate chemistry  
125 (Walker and Kasting, 1992), and includes the canonical long-term carbon cycle fluxes that are  
126 at the heart of current Phanerozoic modelling frameworks (Berner, 2006; Lenton et al., 2018;  
127 Krause et al., 2018), whereby carbon is supplied to the surface system via tectonic degassing;  
128 silicate and carbonate weathering are dependent on global temperature through reaction  
129 kinetics and runoff relationships; and marine carbonate burial depends on  $\text{CaCO}_3$  saturation  
130 state through a power-law relationship, e.g. (Rampino and Caldeira, 2005). A brief summary  
131 of the most important equations and a full model derivation are in the SI. The model is designed  
132 around a preindustrial steady state and we begin our experiments from a steady state in which

133 the tectonic CO<sub>2</sub> input rate is increased to 50% higher than the present day. This raises  
134 atmospheric CO<sub>2</sub> to ~550 ppm.

135

136 Figure 3 shows the response of the model to a calcium sulfate weathering event in which we  
137 test the addition of between 10<sup>13</sup> and 10<sup>14</sup> moles of Ca per year for 1 million years. This is a  
138 maximum estimate intended to test the full scope of system response, and while such large  
139 input events may have occurred at points in Earth history (Shields et al., 2019), recent estimates  
140 of the mass of sulfate liberated during the Himalayan collision have been revised downwards  
141 to around 3 – 4 × 10<sup>12</sup> moles per year over a longer period (Yao et al., 2020). In the model,  
142 over the first 150 kyr of weathering, ocean Ca concentration doubles. This rise in concentration  
143 leads to excess CaCO<sub>3</sub> burial, which reduces ocean alkalinity and drives a transient sea-to-air  
144 flux of CO<sub>2</sub>, raising the atmospheric concentration by up to 200 ppm during the period of  
145 instability. Stability is regained because ocean acidification reduces CaCO<sub>3</sub> burial, and  
146 alkalinity is delivered from enhanced continental weathering in a warmer climate. Although  
147 the high-end of the calcium input scenario in the model results in an unrealistic 80 mM of Ca  
148 after 1 Myr, the peak in CO<sub>2</sub> occurs after only ~150 kyr, when [Ca] is a more modest 20 mM.

149

150 In Figure 4 we test an evaporite deposition event of between 5 × 10<sup>12</sup> and 2 × 10<sup>13</sup> moles per  
151 year for 1 Myr. We cannot test such large amounts of Ca removal as we can for input because  
152 the marine Ca reservoir in our model would be entirely depleted, and the maximal scenario we  
153 test has an output rate in line with the Messinian Salinity Crisis (Blanc, 2006), which is  
154 considered to have removed ~1.4 × 10<sup>19</sup> moles of Ca - sufficient to more than halve the  
155 modern marine Ca reservoir – assuming that 20% of all deposited evaporite (Blanc, 2006) was  
156 in the form of CaSO<sub>4</sub> (gypsum, selenite or anhydrite). Estimates for CaSO<sub>4</sub> deposition rates  
157 during other evaporite giant episodes are comparable, e.g. 1.1 × 10<sup>13</sup> moles per year for 2 Myr  
158 for the early Cretaceous Aptian event (Wortmann and Chernyavsky, 2007). Evaporite  
159 deposition has a more powerful climate impact and cooling effects continue for the duration of  
160 the event, rather than being quickly buffered by changes to continental weathering. This is  
161 because the shelf sea alkalinity budget is resupplied from the large deep ocean reservoir,  
162 somewhat nullifying the reduction in silicate weathering rates caused by climate cooling.  
163 Overall, a maximal evaporite weathering event (Figure 3) might result in a ~200 kyr CO<sub>2</sub> spike  
164 of 50-200 ppm, but the rate of evaporite weathering during the early Cenozoic implies that the  
165 low end of this range is far more likely. In contrast, the Messinian-like forcing we apply results

166 in a ~50 to ~300 ppm reduction in atmospheric CO<sub>2</sub>, which drives ~0.5 to ~6°C of global  
167 cooling in the model.

168

### 169 **The potential role of evaporites in climate forcing and feedbacks**

170 Although it would be tempting to link enhanced evaporite weathering due to Himalayan  
171 collision with short-lived hyperthermal events of the Eocene Epoch, past weathering fluxes are  
172 still too poorly constrained to draw any firm conclusions. Relating these model scenarios  
173 directly to the geological record evidently requires more detailed study.

174 In contrast to major weathering during orogeny, major evaporite deposition drives  
175 stable cooling throughout events, which are better constrained in terms of timing and  
176 magnitude. The first evaporite giants of the Cenozoic Era formed during the stepwise closure  
177 of the Mesopotamian Seaway, which terminated around 13.8 Ma, when the onset of permanent  
178 glaciation of Antarctica caused global sea levels to fall (Bialik et al., 2019). Thick gypsum  
179 deposits formed from ca. 16 Ma (Al-Juboury and McCann, 2008), culminating in the short-  
180 lived Badenian Salinity Crisis (De Leeuw et al., 2010) once the Paratethys Ocean became cut  
181 off at 13.8 Ma (Langhian-Serravalian boundary). Evaporite deposition thus coincided with an  
182 interval of major cooling (Fig. 2), while the relationship between cooling, sea-level fall, basin  
183 restriction and evaporite deposition may have acted as a positive feedback reinforcing cooling.

184 A similar positive feedback can be envisaged towards the end of the Miocene when the  
185 main Tortonian phase of anhydrite deposition in the Red Sea and Gulf of Suez (Bosworth,  
186 2015; Rohais et al., 2016) again accompanied global cooling (Herbert et al., 2016). Similarly,  
187 the expansion of ice cover in Antarctica to near modern levels by 6.0 Ma is considered to have  
188 triggered the Messinian Salinity Crisis (Pérez-Asensio et al., 2013). Messinian cooling was  
189 accompanied by intensification of the Asian Winter Monsoon and resulted in the onset of  
190 ephemeral Northern Hemisphere glaciations between 6.0 Ma and 5.5 Ma (Holbourn et al.,  
191 2018), coinciding with maximal rates of sulfate deposition in the Mediterranean Sea between  
192 5.96 Ma and 5.55 Ma (Cosentino et al., 2013). Total closure of the Mediterranean Sea and  
193 deposition of a thick halite layer followed further sea-level drawdown related to the last major  
194 period of glacial expansion of the Miocene (TG12), which took place around 5.5 Ma (Speranza  
195 et al., 2013). This ‘Messinian Gap’ was then followed by a second, shorter interval of sulfate  
196 deposition between 5.50 and 5.33 Ma (Cosentino et al., 2013).

197 Evaporites contributed conceivably to negative climate feedbacks, too, due to the  
198 common association between evaporite giants, warm climates and rifting. Conversely, a  
199 weakening of this negative feedback due to low seawater sulfate might have exacerbated global

200 warming during mass extinctions, e.g. early Cambrian (Botoman), late Devonian, Permian-  
201 Triassic, Triassic-Jurassic events, which all followed extensive evaporite deposition (Warren,  
202 2010). Prolonged sulfate deposition would also have exacerbated ocean anoxia due to the  
203 oxygen deficit caused by an imbalance between terrestrial sulfide oxidation and marine pyrite  
204 burial, a reversal of the oxygen surplus caused by sulfate weathering during ocean oxygenation  
205 events of the Neoproterozoic Era (Shields et al., 2019).

206

## 207 **Conclusion**

208 Non-steady-state evaporite dynamics have the potential to drive global climate change on long  
209 time scales. Although the magnitude of such effects requires case-by-case study, our purpose  
210 here has been to demonstrate a new climate mechanism, in which the deposition of evaporite  
211 giants, in particular, has the potential to overwhelm the silicate weathering thermostat and force  
212 global cooling either directly or via feedbacks between evaporite deposition, climate change  
213 and ice sheet dynamics.

214

## 215 **Acknowledgements**

216 The authors gratefully acknowledge funding support from a Leverhulme Research Fellowship  
217 (RF-2019-435) and NERC grant NE/P013643/1 (BETR programme) to G.A.S. and a NERC  
218 grant (NE/S009663/1) and University of Leeds Academic Fellowship to B.J.W.M. We also  
219 thank U. Wortmann, O. Bialik and an anonymous reviewer for their constructive comments.



220  
221  
222  
223  
224  
225  
226  
227  
228  
229  
230  
231  
232  
233  
234  
235  
236  
237  
238  
239  
240  
241  
242  
243  
244  
245  
246  
247  
248  
249  
250  
251  
252

## Figure captions

**Figure 1. Delivery and removal of marine calcium and carbonate alkalinity.** The three key weathering types are shown in different colours, where multiple arrows represent molar stoichiometry. Carbonate weathering (blue) transfers calcium and carbonate alkalinity from the continental rock reservoir, and CO<sub>2</sub> from the atmosphere, into the ocean. Carbonate deposition (black) reverses this process, removing alkalinity and calcium and releasing CO<sub>2</sub>. Silicate weathering (purple) transfers calcium from the rock reservoir to the ocean, and transfers two moles of carbon from the atmosphere to the ocean. Evaporite weathering (yellow) transfers only calcium to the ocean. Note that this is a simplification – see the model derivation for all fluxes and processes.

**Figure 2. Cenozoic global average temperature against evaporite events.** Temperature record from Hansen et al. (2013). The postulated period of evaporite weathering is shown as yellow and known deposition events are shown as vertical teal bars. Horizontal blue bars show the existence of ice caps in the northern and southern hemispheres.

**Figure 3. Model predictions for an evaporite weathering event.** A. Calcium sulfate input is imposed for 1Myr. B. Marine calcium concentration increases substantially. C. A pulse of CaCO<sub>3</sub> burial occurs due to increased Ca but is nullified as alkalinity falls. D. Atmospheric CO<sub>2</sub> rises through air-sea exchange as ocean pCO<sub>2</sub> increases. E. Global average surface temperature. Shaded area represents weathering between 10<sup>13</sup> and 10<sup>14</sup> moles per year.

**Figure 4. Model predictions for an evaporite deposition event.** A. Calcium sulfate deposition is imposed for 1Myr. B. Marine calcium concentration decreases substantially. C. A CaCO<sub>3</sub> burial is greatly reduced as [Ca] falls. D. Atmospheric CO<sub>2</sub> falls through air-sea exchange as ocean pCO<sub>2</sub> decreases. E. Global average surface temperature. Shaded area represents deposition between 5 × 10<sup>12</sup> and 2 × 10<sup>13</sup> moles per year.

253

254

255 **References**

256 Al-Juboury, A.I., and McCann, T., 2008, The Middle Miocene Fatha (Lower Fars)

257 Formation, Iraq: *GeoArabia*, v. 13, p. 141–174.

258 Berner, R.A., 1991, A model for atmospheric CO<sub>2</sub> over Phanerozoic time: *American Journal*

259 of Science, v. 291, p. 339–376, doi:10.2475/ajs.291.4.339.

260 Berner, R.A., 2006, GEOCARBSULF: A combined model for Phanerozoic atmospheric O<sub>2</sub>

261 and CO<sub>2</sub>: *Geochimica et Cosmochimica Acta*, doi:10.1016/j.gca.2005.11.032.

262 Berner, R.A., 2012, Jacques-Joseph Ebelmen, the founder of earth system science: *Comptes*

263 Rendus - Geoscience, v. 344, p. 544–548, doi:10.1016/j.crte.2012.08.001.

264 Bialik, O.M., Frank, M., Betzler, C., Zammit, R., and Waldmann, N.D., 2019, Two-step

265 closure of the Miocene Indian Ocean Gateway to the Mediterranean: *Scientific Reports*,

266 v. 9, p. 1–10, doi:10.1038/s41598-019-45308-7.

267 Blanc, P., 2006, Improved modelling of the Messinian Salinity Crisis and conceptual

268 implications: v. 238, p. 349–372, doi:10.1016/j.palaeo.2006.03.033.

269 Bosworth, W., 2015, Geological evolution of the Red Sea: Historical background, review,

270 and synthesis, *in* Rasul, N.M.A. and Stewart, I.C.F. eds., *The Red Sea*, Springer Berlin

271 Heidelberg, p. 45–78, doi:10.1007/978-3-662-45201-1\_3.

272 Cosentino, D., Buchwaldt, R., Sampalmieri, G., Iadanza, A., Cipollari, P., Schildgen, T.F.,

273 Hinnov, L.A., Ramezani, J., Bowring, S.A., and Ambientale, G., 2013, Refining the

274 Mediterranean “Messinian gap” with high-precision U-Pb zircon geochronology,

275 central and northern Italy: , p. 323–326, doi:10.1130/G33820.1.

276 Dal Corso, J., Mills, B.J.W., Chu, D., Newton, R.J., Mather, T.A., Shu, W., Wu, Y., Tong, J.,

277 and Wignall, P.B., 2020, Permo–Triassic boundary carbon and mercury cycling linked

278 to terrestrial ecosystem collapse: *Nature Communications*, v. 11, p. 1–9,

279 doi:10.1038/s41467-020-16725-4.

280 Greene, S.E., Ridgwell, A., Kirtland Turner, S., Schmidt, D.N., Pälike, H., Thomas, E.,

281 Greene, L.K., and Hoogakker, B.A.A., 2019, Early Cenozoic decoupling of climate and

282 carbonate compensation depth trends: *Paleoceanography and Paleoclimatology*, v. 34, p.

283 930–945, doi:10.1029/2019PA003601.

284 Halevy, I., Peters, S.E., and Fischer, W.W., 2012, Sulfate burial constraints on the

285 Phanerozoic sulfur cycle: *Science*, v. 337, p. 331-334, doi:10.1126/science.12.20224.  
286 Hansen, J., Sato, M., Russell, G., and Kharecha, P., 2013, Climate sensitivity, sea level and  
287 atmospheric carbon dioxide: *Philosophical Transactions of the Royal Society A:*  
288 *Mathematical, Physical and Engineering Sciences*, doi:10.1098/rsta.2012.0294.  
289 Herbert, T.D., Lawrence, K.T., Tzanova, A., Peterson, L.C., Caballero-Gill, R., and Kelly,  
290 C.S., 2016, Late Miocene global cooling and the rise of modern ecosystems: *Nature*  
291 *Geoscience*, v. 9, doi:10.1038/NGEO2813.  
292 Holbourn, A.E., Kuhnt, W., Lübbers, J., Andersen, N., and Clemens, S.C., 2018, Late  
293 Miocene cooling and intensification of southeast Asian winter monsoon: *Nature*  
294 *Communications*, doi:10.1038/s41467-018-03950-1.  
295 Krause, A.J., Mills, B.J.W., Zhang, S., Planavsky, N.J., Lenton, T.M., and Poulton, S.W.,  
296 2018, Stepwise oxygenation of the Paleozoic atmosphere: *Nature Communications*,  
297 doi:10.1038/s41467-018-06383-y.  
298 De Leeuw, A., Bukowski, K., Krijgsman, W., and Kuiper, K.F., 2010, Age of the Badenian  
299 salinity crisis; Impact of Miocene climate variability on the circum-mediterranean  
300 region: *Geology*, v. 38, p. 715–718, doi:10.1130/G30982.1.  
301 Lenton, T.M., Daines, S.J., and Mills, B.J.W., 2018, COPSE reloaded: An improved model of  
302 biogeochemical cycling over Phanerozoic time: *Earth-Science Reviews*, v. 178, p. 1–28,  
303 doi:10.1016/j.earscirev.2017.12.004.  
304 Mandić, O., Sant, K., Kallanxhi, M., Ćorić, S., Theobalt, D., Grunert, P., Leeuw, A. De, and  
305 Krijgsman, W., 2019, Integrated bio-magnetostratigraphy of the Badenian reference  
306 section Ugljevik in southern Pannonian Basin - implications for the Paratethys history (   
307 middle Miocene , Central Europe ): *Global and Planetary Change*, v. 172, p. 374–395,  
308 doi:10.1016/j.gloplacha.2018.10.010.  
309 Meilijson, A., Hilgen, F., Sepulveda, J., Steinberg, J., Fairbank, V., Flecker, R., Waldmann,  
310 N.D., Spaulding, S.A., Bialik, O., Boudinot, F.G., Illner, P., and Makovsky, Y., 2019,  
311 Chronology with a pinch of salt: Integrated stratigraphy of Messinian evaporites in the  
312 deep Eastern Mediterranean reveals long-lasting halite deposition during Atlantic  
313 connectivity: *Earth Science Reviews*, v. 194, 374-398,  
314 doi:10.1016/j.earscirev.2019.05.011.  
315 Mills, B.J.W., Krause, A.J., Scotese, C.R., Hill, D.J., Shields, G.A., and Lenton, T.M., 2018,  
316 Modelling the long-term carbon cycle, atmospheric CO<sub>2</sub>, and Earth surface temperature  
317 from late Neoproterozoic to present day: *Gondwana Research*, v. 67, p. 172–186,  
318 doi:10.1016/j.gr.2018.12.001.

319 Pérez-Asensio, J.N., Aguirre, J., Jiménez-Moreno, G., Schmiedl, G., and Civis, J., 2013,  
320 Glacioeustatic control on the origin and cessation of the Messinian salinity crisis: *Global*  
321 *and Planetary Change*, v. 111, p. 1–8, doi:10.1016/j.gloplacha.2013.08.008.

322 Rampino, M.R., and Caldeira, K., 2005, Major perturbation of ocean chemistry and a  
323 “Strangelove Ocean” after the end-Permian mass extinction: *Terra Nova*, v. 17, p. 554–  
324 559, doi:10.1111/j.1365-3121.2005.00648.x.

325 Rohais, S., Barrois, A., Colletta, B., and Moretti, I., 2016, Pre-salt to salt stratigraphic  
326 architecture in a rift basin : insights from a basin-scale study of the Gulf of Suez (Egypt):  
327 *Arabian Journal of Geosciences*, doi:10.1007/s12517-016-2327-8.

328 Sarmiento, J.L., and Toggweiler, J.R., 1984, A new model for the role of the oceans in  
329 determining atmospheric pCO<sub>2</sub>: *Nature*, v. 308i, p. 621–624.

330 Shields, G.A., Mills, B.J.W., Zhu, M., Raub, T.D., Daines, S.J., and Lenton, T.M., 2019,  
331 Unique Neoproterozoic carbon isotope excursions sustained by coupled evaporite  
332 dissolution and pyrite burial: *Nature Geoscience*, doi:10.1038/s41561-019-0434-3.

333 Speranza, G., Cosentino, D., Tecce, F., and Faccenna, C., 2013, Paleoclimate reconstruction  
334 during the Messinian evaporative drawdown of the Mediterranean Basin: Insights from  
335 microthermometry on halite fluid inclusions: *Geochemistry, Geophysics, Geosystems*, v.  
336 14, p. 5054–5077, doi:10.1002/2013GC004946.

337 Walker, J.C.G., Hays, P.B., and Kasting, J.F., 1981, A negative feedback mechanism for the  
338 long-term stabilization of Earth’s surface temperature: *Journal of Geophysical Research*,  
339 v. 86, p. 9776, doi:10.1029/JC086iC10p09776.

340 Walker, J.C.G., and Kasting, J.F., 1992, Effects of fuel and forest conservation on future  
341 levels of atmospheric carbon dioxide: *Global and Planetary Change*, v. 5, p. 151–189,  
342 doi:10.1016/0921-8181(92)90009-Y.

343 Warren, J.K., 2010, Evaporites through time: Tectonic, climatic and eustatic controls in  
344 marine and nonmarine deposits: *Earth-Science Reviews*,  
345 doi:10.1016/j.earscirev.2009.11.004.

346 Wortmann, U.G., and Chernyavsky, B.M., 2007, Effect of evaporite deposition on Early  
347 Cretaceous carbon and sulphur cycling: *Nature*, v. 446, p. 654–656,  
348 doi:10.1038/nature05693.

349 Wortmann, U.G., and Paytan, A., 2012, Rapid variability of seawater chemistry over the past  
350 130 million years: *Science*, v. 337, p. 334–336, doi:10.1126/science.1220656.

351 Yao, W., Paytan, A., Griffith, E.M., Martínez-Ruiz, F., Markovic, S., and Wortmann, U.G.,  
352 2020, A revised seawater sulfate S-isotope curve for the Eocene: *Chemical Geology*, v.

353 532, p. 119382, doi:10.1016/j.chemgeo.2019.119382.  
354 Zachos, J.C., Dickens, G.R., and Zeebe, R.E., 2008, An early Cenozoic perspective on  
355 greenhouse warming and carbon-cycle dynamics: *Nature*, v. 451, p. 279–283,  
356 doi:10.1038/nature06588.  
357 Zachos, J., Pagani, M., Sloan, L., Thomas, E., and Billups, K., 2001, Trends, Rhythms, and  
358 Aberrations in Global Climate 65 Ma to Present: *Discovery Service para UNAM:*  
359 *Science*, v. 292, p. 686–693, doi:10.1126/science.1059412.  
360 Zeebe, R.E., and Tyrrell, T., 2019, History of carbonate ion concentration over the last 100  
361 million years II: Revised calculations and new data: *Geochimica et Cosmochimica Acta*,  
362 v. 257, p. 373-392, doi:10.1016/j.gca.2019.02.041.  
363

Carbonate weathering

Silicate weathering

Evaporite weathering

Rock  
reservoir

$\text{CO}_2$

$\text{Ca}^{2+}$

$\text{HCO}_3^-$

$\text{CaCO}_3$

Carbonate deposition

